Demonstration of suppressed phonon tunneling losses in phononic bandgap shielded membrane resonators for high-Q optomechanics

Yeghishe Tsaturyan,[1] Andreas Barg,[1] Anders Simonsen,[1] Luis Guillermo Villanueva,[2] Silvan Schmid,[2] Albert Schliesser,[1,*] and Eugene S. Polzik[1,3]

[1] *Niels Bohr Institute, Copenhagen University, Blegdamsvej 17, 2100 Copenhagen, Denmark*
[2] *Department of Micro- and Nanotechnology, Technical University of Denmark, 2800 Kongens Lyngby, Denmark*
[3]*polzik@nbi.dk*

*albert.schliesser@nbi.dk

Abstract: Dielectric membranes with exceptional mechanical and optical properties present one of the most promising platforms in quantum optomechanics. The performance of stressed silicon nitride nanomembranes as mechanical resonators notoriously depends on how their frame is clamped to the sample mount, which in practice usually necessitates delicate, and difficult-to-reproduce mounting solutions. Here, we demonstrate that a phononic bandgap shield integrated in the membrane's silicon frame eliminates this dependence, by suppressing dissipation through phonon tunneling. We dry-etch the membrane's frame so that it assumes the form of a cm-sized bridge featuring a 1-dimensional periodic pattern, whose phononic density of states is tailored to exhibit one, or several, full band gaps around the membrane's high-Q modes in the MHz-range. We quantify the effectiveness of this phononic bandgap shield by optical interferometry measuring both the suppressed transmission of vibrations, as well as the influence of frame clamping conditions on the membrane modes. We find suppressions up to 40 dB and, for three different realized phononic structures, consistently observe significant suppression of the dependence of the membrane's modes on sample clamping—*if* the mode's frequency lies in the bandgap. As a result, we achieve membrane mode quality factors of 5×10^6 with samples that are tightly bolted to the 8 K-cold finger of a cryostat. $Q \times f$-products of 6×10^{12} Hz at 300 K and 14×10^{12} Hz at 8 K are observed, satisfying one of the main requirements for optical cooling of mechanical vibrations to their quantum ground-state.

References and links

1. S. S. Verbridge, J. M. Parpia, R. B. Reichenbach, L. M. Bellan, and H. G. Craighead, "High quality factor resonance at room temperature with nanostrings under high tensile stress," J. Appl. Phys. **99**, 124304 (2006).

2. Q. P. Unterreithmeier, T. Faust, and J. P. Kotthaus, "Damping of nanomechanical resonators," Phys. Rev. Lett. **105**, 027205 (2010).
3. S. Schmid, K. D. Jensen, K. H. Nielsen, and A. Boisen, "Damping mechanisms in high-Q micro and nanomechanical string resonators," Phys. Rev. B **84**, 165307 (2011).
4. B. M. Zwickl, W. E. Shanks, A. M. Jayich, C. Yang, C. Bleszynski Jayich, J. D. Thomson, and J. G. E. Harris, "High quality mechanical and optical properties of commercial silicon nitride membranes," Appl. Phys. Lett. **92**, 103125 (2008).
5. D. J. Wilson, C. A. Regal, S. B. Papp, and H. J. Kimble, "Cavity optomechanics with stoichiometric SiN films," Phys. Rev. Lett. **103**, 207204 (2009).
6. T. P. Purdy, R. W. Peterson, P.-L. Yu, and C. A. Regal, "Cavity optomechanics with Si_3N_4 membranes at cryogenic temperatures," New J. Phys. **14**, 115021 (2012).
7. S. Chakram, Y. S. Patil, L. Chang, and M. Vengalattore, "Dissipation in ultrahigh quality factor SiN membrane resonators," arXiv:1311.1234 (2013).
8. J. D. Thompson, B. M. Zwickl, A. M. Jayich, F. Marquardt, S. M. Girvin, and J. G. E. Harris, "Strong dispersive coupling of a high finesse cavity to a micromechanical membrane," Nature **452**, 72–75 (2008).
9. T. P. Purdy, R. W. Peterson, and C. A. Regal, "Observation of radiation pressure shot noise on a macroscopic object," Science **339**, 801–804 (2013).
10. T. P. Purdy, P.-L. Yu, R. W. Peterson, N. S. Kampel, and C. A. Regal, "Strong optomechanical squeezing of light," Phys. Rev. X **3**, 031012 (2013).
11. M. Karuza, C. Biancofiore, M. Bawaj, C. Molinelli, M. Galassi, R. Natali, P. Tombesi, G. Di Giuseppe, and D. Vitali, "Optomechanically induced transparency in a membrane-in-the-middle setup at room temperature," Phys. Rev. A **88** (2013).
12. T. Bagci, A. Simonsen, S. Schmid, L. G. Villanueva, E. Zeuthen, J. Appel, J. M. Taylor, A. Sørensen, K. Usami, A. Schliesser, and E. S. Polzik, "Optical detection of radio waves through a nanomechanical transducer," arXiv:1307.3467 (2013).
13. R. W. Andrews, R. W. Peterson, T. P. Purdy, K. Cicak, R. W. Simmonds, C. A. Regal, and K. W. Lehnert, "Reversible and efficient conversion between microwave and optical light," arXiv:1310.5276 (2013).
14. K. Hammerer, M. Aspelmeyer, E. Polzik, and P. Zoller, "Establishing Einstein-Poldosky-Rosen channels between nanomechanics and atomic ensembles," Phys. Rev. Lett. **102**, 020501 (2009).
15. K. Hammerer, K. Stannigel, C. Genes, P. Zoller, P. Treutlein, S. Camerer, D. Hunger, and T. W. Hänsch, "Optical lattices with micromechanical mirrors," Phys. Rev. A **82**, 021803 (2010).
16. D. R. Southworth, R. A. Barton, S. S. Verbridge, B. Ilic, A. D. Fefferman, H. G. Craighead, and J. M. Parpia, "Stress and silicon nitride: A crack in the universal dissipation of glasses," Phys. Rev. Lett. **102**, 225503 (2009).
17. P.-L. Yu, T. P. Purdy, and C. A. Regal, "Control of material damping in high-Q membrane microresonators," Phys. Rev. Lett. **108**, 083603 (2012).
18. T. Faust, J. Rieger, M. J. Seitner, J. P. Kotthaus, and E. M. Weig, "Signatures of two-level defects in the temperature-dependent damping of nanomechanical silicon nitride resonators," arXiv:1310.3671 (2013).
19. V. P. Adiga, B. Ilic, R. A. Barton, I. Wilson-Rae, H. G. Craighead, and J. M. Parpia, "Approaching intrinsic performance in ultra-thin silicon nitride drum resonators," J. Appl. Phys. **112**, 064323 (2012).
20. C. Enss and S. Hunklinger, *Low Temperature Physics* (Springer, 2005), Chap. 9, pp. 283–341.
21. I. Wilson-Rae, "Intrinsic dissipation in nanomechanical resonators due to phonon tunneling," Phys. Rev. B **77**, 245418 (2008).
22. A. Jockel, M. T. Rakher, M. Korppi, S. Camerer, D. Hunger, M. Mader, and P. Treutlein, "Spectroscopy of mechanical dissipation in micro-mechanical membranes," Appl. Phys. Lett. **99**, 143109 (2011).
23. M. Maldovan and E. L. Thomas, *Periodic Materials and Interference Lithography for Photonics, Phononics and Mechanics* (Wiley-VCH, 2009), Chap. 7, pp. 183–213.
24. M. Maldovan, "Sound and heat revolutions in phononics," Nature **503**, 209–217 (2013).
25. T. P. Mayer Alegre, A. Safavi-Naeini, M. Winger, and O. Painter, "Quasi-two-dimensional optomechanical crystals with a complete phononic bandgap," Opt. Express **19**, 5658–5669 (2011).
26. P.-L. Yu, K. Cicak, N. S. Kampel, Y. Tsaturyan, T. P. Purdy, R. W. Simmonds, and C. A. Regal, "A phononic bandgap shield for high-*q* membrane microresonators," Appl. Phys. Lett. **104**, 023510 (2014).
27. A. Khelif, B. Aoubiza, S. Mohammadi, A. Adibi, and V. Laude, "Complete band gaps in two-dimensional phononic crystal slabs," Phys. Rev. E **74**, 046610 (2006).
28. N. W. Ashcroft and N. D. Mermin, *Solid State Physics*, 1st ed. (Cengage Learning, 1976).
29. G. S. May and S. M. Sze, *Fundamentals of Semiconductor Fabrication*, 1st ed. (John Wiley, 2003).
30. A. H. Safavi-Naeini and O. Painter, "Design of optomechanical cavities and waveguides on a simultaneous bandgap phononic-photonic crystal slab," Opt. Express **18**, 14926–14943 (2010).

1. Introduction

Highly stressed nano-strings [1–3] and -membranes [4–6] of stoichiometric silicon nitride (Si_3N_4) possess mechanical resonances at MHz frequencies with extraordinarily low dissipation, reaching Q-factors up to 5×10^7 [7] and Q-frequency-products well beyond 10^{13}. In combination with large zero-point motion ($\mathcal{O}(1 \text{ fm})$), this renders them a promising platform for experiments in quantum optomechanics. Indeed, since the pioneering experiment of Thompson *et al.* [8], who showed how nanomembranes can be coupled efficiently to an optical mode using the so-called membrane-in-the-middle approach, they have been employed for a number of striking demonstrations of optomechanical physics. These include strong cooling [5,8], observation of radiation pressure quantum backaction [9], squeezing [10], optomechanically induced transparency [11] and the first proof-of-principle implementations of mechanically resonant electro-optical transducers [12,13].

These ongoing, and further proposed audacious experiments [14,15], all require the highest possible mechanical Q. Several recent studies [16–19] indicate that an internal loss mechanism, possibly coupling to two-level systems [20], sets the ultimate upper bound for the Q that can be attained. However, losses due to phonon tunneling [21] from the membrane mode into the modes of its frame often limit the Q in practice [3,5,22]. This is due to the fact that the clamping of the frame to the sample mount usually induces strong damping of the frame modes. The membrane modes coupled to the frame modes thus suffer strong dissipation. The dissipation induced by this coupling can sometimes be evaded by minimizing the contact of the frame with the sample mount (suppressing the loss of the *frame* modes) [3,6], but reduced stability, control and—important for cryogenic experiments—thermal anchoring render this approach less attractive.
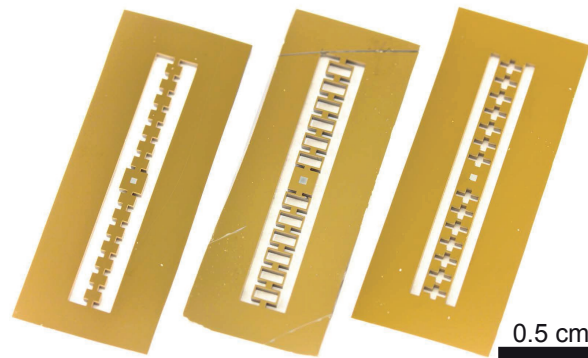

Fig. 1. Photographs of SiN membranes held in the center of a periodically modulated silicon bridge. The silicon appears golden as the entire wafer has been coated with SiN, but it is etched from the backside only in the center to release the membrane. From left to right, three different unit cells of the periodic pattern were chosen, which we refer to as the drum structure, hollow drum structure and cross structure, respectively. The periodic arrangement of these cells leads to a bandgap in the phonon density of states, whose frequency span contains the membranes' mechanical modes of interest.

Instead, we choose here to tailor the density of phononic states in the membrane frame by patterning it with a phononic structure [23,24]. The latter are employed in science and technology at all possible frequency and length scales, including earthquake protections, but also in surface acoustic wave devices, and most recently, optomechanical structures [25,26]. In our case, we achieve a modulation of the phononic potential landscape by periodically removing parts of the elastic material (silicon), which gives rise to a band gap in the phonon dispersion.

The thin ($\sim 500\,\mu$m) frame naturally constitutes a slab geometry, but in contrast to previous studies [27], we choose to adapt one-dimensional structures—essentially thin, long bridges—as a space-saving alternative with ample design flexibility, enabling particularly wide bandgaps (Fig. 1).

2.   Simulations

In this work we study three different quasi-one-dimensional phononic crystal structures shown in Fig. 1, each with their own characteristic features. The drum structure, mimicking a double mass-spring system with alternating masses [26], has three consecutive bandgaps in the frequency range of 2–4 MHz. The hollow drum structure has three bandgaps as well, however, in a lower frequency range, e.g. between 0.7 –2.4 MHz. Finally, the cross structure has one large bandgap in the range of 2.5–3.5 MHz. An overview of the band diagrams for these structure is shown in Fig. 2.
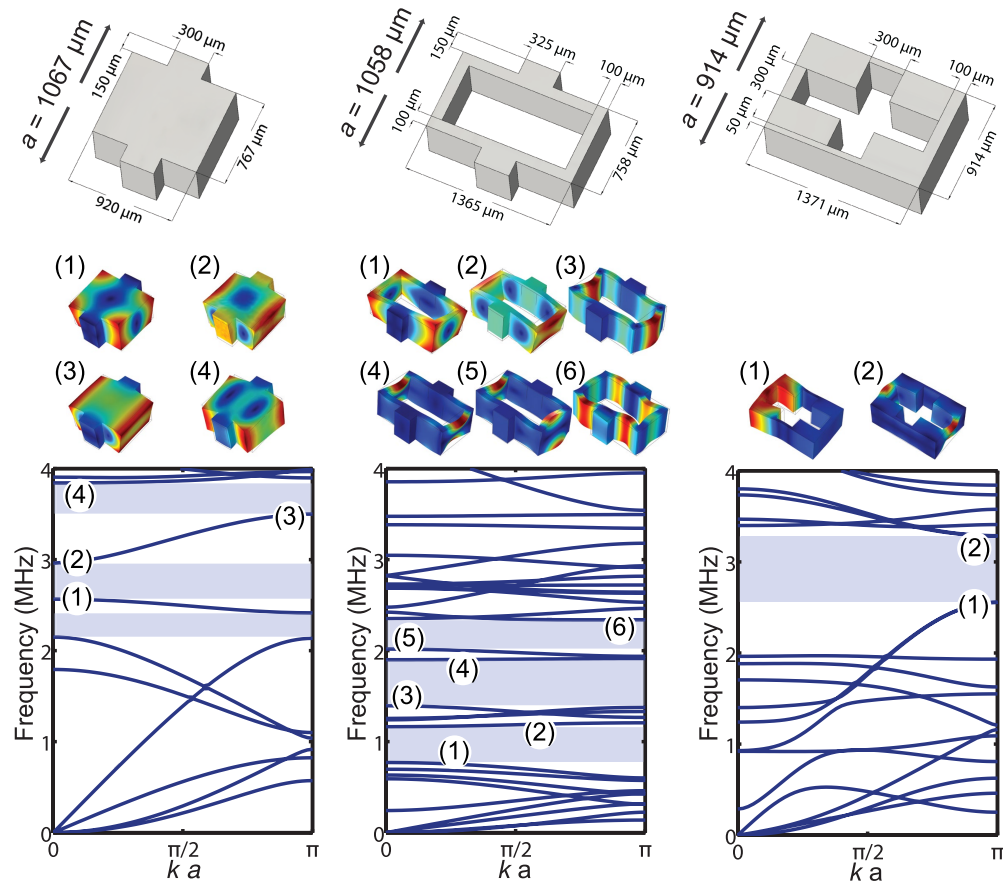

Fig. 2. Unit cells (top) and band diagrams (bottom) for the drum, hollow drum and cross structures (left to right). The bandgaps relevant for our devices have been highlighted. Central row shows displacement patterns of the unit cells, as simuated numerically, for the modes at the band edges labeled in the band diagrams. The dimensions for the unit cells presented above lay the basis for the photomasks, used in the fabrication process. Also, the unit cell sizes a are indicated (top).

The calculations of the band diagrams have been carried out in COMSOL through eigenfrequency analysis, employing Bloch-Floquet periodicity [28] at the boundaries of the unit cells, which are the elements of periodicity. An infinite structure with periodicity a (e.g. the size of the unit cell in the direction of propagation, cf. Fig. 2) is assumed and the eigenfrequencies for different wavenumbers are calculated.

The structures have been optimized based on fabrication constraints and for a large relative bandgap size, $f_c/\Delta f$, where f_c is the center-frequency of the bandgap and Δf is the bandgap size. Importantly, we have found that wide bandgaps can only be obtained with vertical side-walls of the holes, necessitating a physical dry etch process for patterning the silicon slab. Full 3D simuations without restrictions with respect to the polarization of the propagating waves have been performed (cf. Fig. 2), thus the bandgaps obtained are complete phononic bandgaps, with no propagating modes existing in these frequency regions.

Once the band diagrams have been calculated, the membrane mode of interest can be positioned inside a given bandgap, by adjusting the membrane size. For high-stress membrane resonators of square geometry the eigenfrequencies are given by $f_{n,m} = \sqrt{\frac{\sigma}{4\rho L^2}(n^2 + m^2)}$, where σ is the tensile stress (~ 1.14 GPa for our devices), ρ is the density of silicon nitride, L is the side length of a square membrane and (n,m) indicate the number of antinodes of a given membrane mode. The typical membrane size for our devices is $L \sim 300\ \mu$m.

By introducing a defect in the phononic structures, thus breaking the periodicity, vibrations at certain frequencies are confined within the defect, and, reciprocally, the defect is shielded from outside vibrations. Our devices have between 5 and 7 unit cells between the defect and the frame (see Fig. 1), the *defect* being the membrane and the silicon in its immediate vicinity (i.e. the "island" in the middle of the bridge, which includes the membrane). The *bridge*, consisting of the phononic structure and the defect in the middle, is thus ~ 14 mm long for all our devices.

Since our work is aimed at, but certainly not limited to, applications in cavity optomechanics, stable positioning of the bridge is of high importance. For the least rigid devices, the hollow drum structures, we estimate the mean square displacement of the fundamental mode of the bridge to be $\sqrt{\langle x^2 \rangle} \approx 0.92$ pm at 6.2 kHz from the equipartition relation $k_B T = m_{\text{eff}}\Omega_m^2 \langle x^2 \rangle$. Here k_B is the Boltzmann constant, $T = 300$ K, and m_{eff} is half of the physical mass of the bridge. This estimate is in fair agreement with the measured displacement of ~ 2 pm. The fundamental mode frequencies for the drum and cross structures are 11 kHz and 13 kHz, respectively.

3. Fabrication

Our devices are fabricated in six steps (see Fig. 3). We begin with low-pressure chemical vapor deposition (LPCVD) of 50 nm stoichiometric silicon nitride (SiN) on a 500 μm silicon wafer. The membranes are defined by the first photolithography step on the back-side of the wafer and the developed regions are etched by reactive ion etching (RIE), opening quadratic windows in the SiN on the wafer's backside. The photoresist is removed and the wafer is stripped of its native silicon oxide by a buffered hydrofluoric acid (BHF) dip, as a preparation for the subsequent KOH etching [29]. The square membranes are released during the KOH etch through the entire thickness of the wafer.

In the second step of photolithography the phononic structure is defined on the front-side of the wafer. The back-side of the wafer is therefore bonded to a carrier wafer using crystalbond (a water soluble mounting adhesive) and etched all the way through using deep reactive ion etching (DRIE), ensuring vertical sidewalls within $\sim 1°$. Heat removal, partly ensured by back-side gas cooling of the support wafer, is crucial during the entire etching process. Therefore,

in order to prevent burning of the photoresist, the etching is done in 10 min steps. After DRIE, the wafer is placed in 80°C water for 20-30 min to dissolve the crystalbond and thus remove the carrier wafer. Finally, the photoresist is removed from the wafer using an overnight acetone bath, as well as 10-20 min of low-power oxygen plasma.
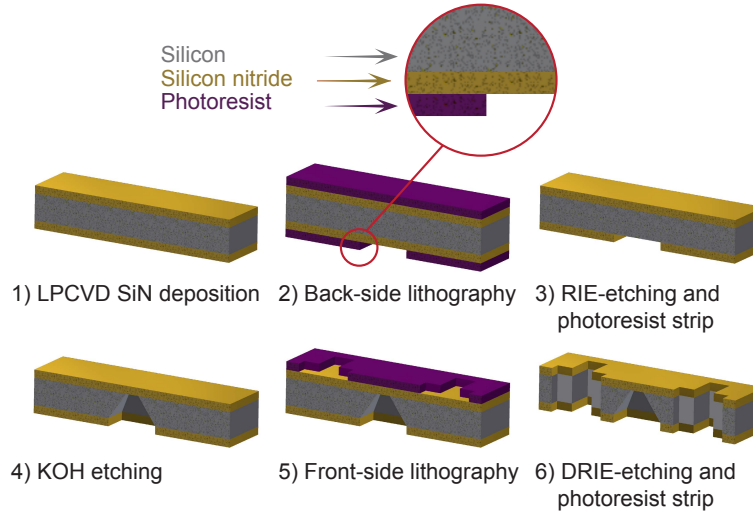

Fig. 3. Illustration of the fabrication process flow. The inset in step 2 shows a cross-sectional view of the wafer after the first lithography step. Prior to photoresist (AZ 5214-E) removal, the wafer is exposed to chemically active plasma, removing silicon nitride and silicon ($\sim 1 \ \mu$m combined thickness) in regions with photoresist openings. In the second step of photolithography we use a thicker layer of photoresist (AZ 4562), in order to protect the SiN membranes during the DRIE.

4. Optical characterization of the phononic bandgap support

The mechanical response of our devices is characterized using an optical interferometer. To that end, the light of a stable laser ($\lambda = 1064$ nm) is reflected off a selected, $\sim 14 \ \mu$m large spot on the sample. The phase of the reflected light is measured by comparing it with the phase of a reference light beam in a high-bandwidth InGaAs balanced homodyne receiver (0-75 MHz). The low-frequency part of the receiver's signal is used to stabilize the reference light's phase, by displacing a mirror in the reference arm of the interferometer. This ensures measurement of the phase quadrature of the light returned from the sample. The recorded phase quadrature is calibrated to a displacement of the probed sample area, by modulating the position of the mirror in the reference arm, at a fixed frequency, with a known amplitude. In that manner, variations of the amount of light returned from the sample, interferometric contrast etc. are eliminated from the signal.

To map out the phononic bandgap we perform response measurements, i. e., the sample is mounted to a sample holder which can be actuated (in the direction perpendicular to the plane of the sample slab) using a piezoelectric transducer. The sample holder is designed so that the phononic bridge can swing freely. We measure the displacement response of the sample in several different spots using a network analyser whose output is fed to the piezo transducer, and whose input is provided by the homodyne receiver. In particular, we compare the response measured at several spots on the frame (outside the bridge) and the defect region (in the center of the bridge, surrounding the membrane), see Fig. 4. In the context of response measurements

the membrane is not part of the defect. Measurements from several spots are averaged in order to minimize the influence of strongly localized modes of the silicon structure. For a reference measurement, the (apparent) displacements of the frame are recorded with the actuation disabled. With the used light powers of ~ 3 mW, this reference trace reveals a shot noise limited sensitivity of 10 fm/$\sqrt{\text{Hz}}$ for the displacement measurements.

First, we consider the response of a cross structure device. Contrary to other measurements the sample was "glued" to a spacer (e.g. bare silicon frame) using double-sided tape and subsequently attached to a piezoelectric transducer. We observe a significant drop in the average response measured on the defect in the frequency range of 2.4–3.2 MHz, reaching up to 40 dB suppression as compared to the frame response (see Fig. 4(a)). Comparing the observed bandgap to the predicted (see Fig. 2), we find that the bandgap sizes and center frequencies coincide to within $\sim 10\%$.
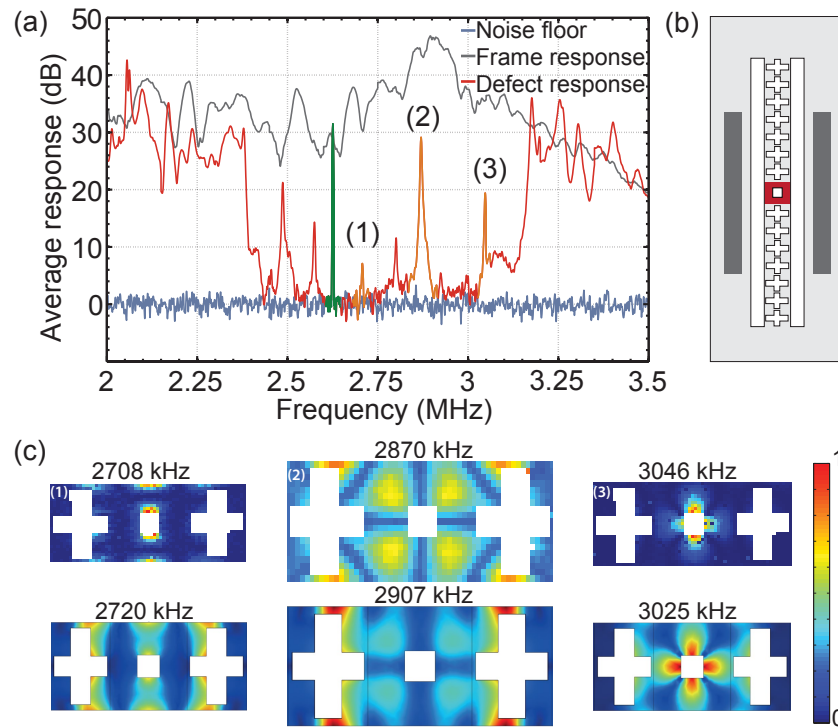

Fig. 4. a) Measurement of the driven response on the defect and the frame, and the non-driven response on the defect. The data constitutes an average of 29 measurement points on the defect and the frame and has been normalized to a trace without actuation (optical shot noise, 0 dB). A calibration peak is positioned around 2.6 MHz (green). b) Illustration of a cross structure device, with the measured regions on the frame (gray) and defect (red) highlighted. c) Comparison of measured (top row) and simulated (bottom row) defect modes, indicated in the response spectrum. The colors indicates the magnitude of vertical displacement.

A small number of sharp resonances is observed in the bandgap. By scanning the probing spot over the sample surface, thus mapping the spatial mode profile of the response at three different resonance frequencies, we identify these as *defect modes*, i.e. localized eigenmodes of the defect. A comparison with a simulation of the device shows good agreement between

several measured and simulated defect modes, with the resonance frequencies differing by a few tens of kilohertz (see Fig. 4(c)). While the remaining defect modes were also measured, we were not able to reproduce the exact frequencies and/or spatial mode profiles, which we attribute to the geometrical differences between the simulated and real device. Note that cooling of the membrane modes can shift their frequencies by several tens of kilohertz. Therefore, being able to predict the defect modes is important for measurements at cryogenic temperatures, in order to avoid steering a membrane mode into potentially detrimental defect modes.

5. Effect of phononic bandgap support on membrane modes

Next, we study the effect of the phononic bandgaps of two shield designs (cross and hollow drum structure, see Fig. 2) on the mechanical quality factors of the membranes. More specifically, we investigate the suppression of membrane losses due to clamping of the frame. For these measurements, performed at room temperature and low pressure ($\lesssim 3 \times 10^{-6}$ mbar), we design a small aluminum sample holder, with a removable cover, that allows tight clamping of the samples frame—while we make sure that the bridge can swing freely. For comparison, we also measure the membrane mode's Q when the sample is free-standing, i.e. resting on the sample mount under its own gravitational weight only. These two configurations will be referred to as *clamped* and *unclamped*.

Due to the high quality factor of the membrane modes, their Q is determined using ringdown measurements. The membrane motion is excited by a actuating the piezoelectric transducer below the sample holder. When the optically measured displacement amplitude reaches a value close to its maximum, the actuation is switched off and the ringdown of the oscillations is recorded. We use small incident light powers on the sample, typically below 200 μW. A small number of high-Q modes inside the phononic bandgap required a more direct actuation, which was realised using optical forces. The incident light power was increased to 2 mW, and modulated in amplitude, thereby exciting the modes optically. Again, the actuation is switched off and the ringdown recorded. We have verified that the increase in light power doesn't affect the quality factors of the membrane modes. For each membrane, we have measured 11 mechanical modes, ranging from the fundamental to the (3,3) mode. The results of these measurements are shown in Fig. 5, along with response measurements of the bridge as described previously.

Both structures show suppression up to 40 dB within the phononic bandgaps. For the cross structure device we find good agreement with the predicted bandgap, while for the hollow drum structure only the first two bandgaps overlap with the simulation (see Fig. 2). In fact, all bandgaps are shifted down in frequency, compared to the simulated band diagrams. It is well known that by reducing the width of the connector pieces of a unit cell, the low frequency band can be pushed further down [30]. In case of the cross structure, the connector pieces corresponds to the 50 μm and 100 μm thin connections perpendicular to and in the direction of propagation. By examining the devices under a microscope we indeed find that these connections can be up to $\sim$ 15% thinner than predicted. For the cross structure we find that the (2,2), as well as the (1,3) and (3,1) modes, are within the bandgap, while for the hollow drum structure the first four mechanical modes are distributed among three bandgaps. In both cases we observe that modes outside the bandgap have predominantly lower quality factors clamped versus unclamped, as one would have expected. As shown in Fig. 5(b), a majority of the membrane modes outside the bandgap are significantly affected by the clamping of the frame. In-bandgap modes, however, are virtually unaffected by the clamping of the substrate, independent of the membrane mode. These initial results already suggest that the bandgap does in fact have an effect on phonon tunneling losses of the membrane modes.
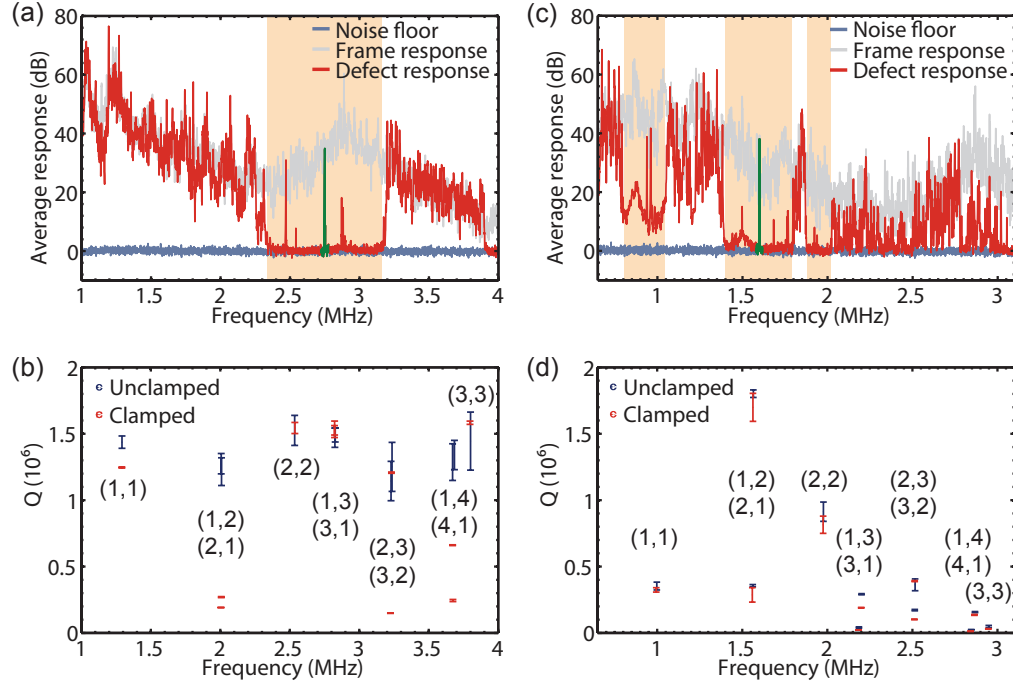
Fig. 5. The response measurements of a cross structure (a-b) and a hollow drum structure device (c-d), accompanied with the mechanical Q-factors. The error bars for the quality factors are the standard deviation of all measured ringdowns for a given mode (typically 20 ringdown measurements for each mode). The response data is an average of 8 measurement points on the defect and the frame. The regions assumed to be the phononic bandgaps are shown in orange, while the calibration peak is indicated in green. The labels in (b) and (d) indicate the membrane modes. For the two devices the membrane sizes are (b) $L \sim 290 \, \mu$m and (d) $L \sim 370 \, \mu$m.

Yet another distinction between the in- and out-of-bandgap modes, and a supporting indication of the successful decoupling of the membrane from the environment, is found in a measurement similar to the one reported by Jöckel *et al.* [22]. More specifically, we consider the frequency dependence of the quality factors, by heating the sample with an electric heater in the sample holder. After each temperature change, we wait 5–10 minutes, in order for the sample to reach thermal equilibrium, as well as the pressure to stabilize. We measure the (2,2) modes of two cross structure devices, with the membrane mode inside and outside the bandgap, respectively. As shown in Fig. 6, the mode outside the bandgap exhibits large dips within a few kilohertz, while the quality factor of the in-bandgap mode is constant. The narrow "resonances" can be explained by the fact that the whole sample is being heated, resulting in the membrane modes moving up in frequency and the frame modes being shifted to lower frequencies [22]. By tuning the membrane mode into a frame mode the quality factor drops significantly. The density of the frame modes (sampled by the membrane in the defect) is strongly suppressed by a phononic bandgap support, therefore such resonant dips are not observed in this case. While it is conceivable that no frame modes existed in the frequency region probed by the in-bandgap mode, even if the bandgap was ineffective, it is unlikely given an average density of modes of approximately 1 per 6 kHz in the relevant frequency range.
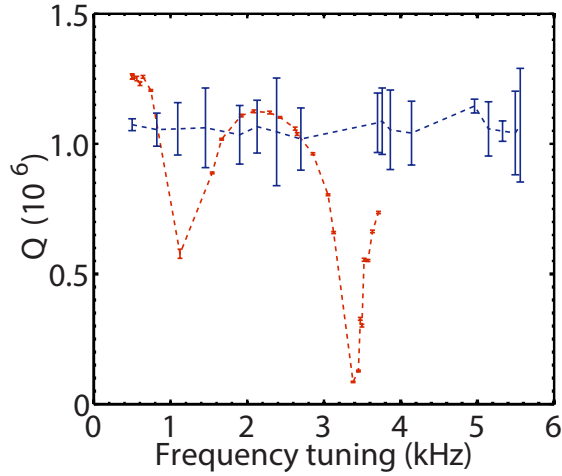
Fig. 6. Frequency dependence of the Q-factor for a (2,2) inside (blue) and outside (red) a phononic bandgap. The change in frequency is induced by a temperature sweep from 303 K to 319 K (in-bandgap mode) and 326 K (mode outside the bandgap). The starting frequencies for the in-bandgap mode is $f_0 = 2.811$ MHz and $f_0 = 3.022$ MHz for the mode outside the bandgap.

Finally, as the main result of our work, we present a large compilation of quality factors of the membrane modes, measured on seven different devices, with phononic bridges of all three types shown in Fig. 1 and membrane sizes ranging from ~ 270 μm to ~ 370 μm. We separate the in-bandgap modes from the membrane modes outside the bandgap and consider their Q-dependence on clamping. Figure 7 clearly shows that modes inside the bandgap are lined up on the diagonal and are thus unaffected by the clamping of the substrate, while modes outside the bandgap are scattered across the measured landscape. By measuring a large number of membrane modes, we have thus established the effectivity of the phononic bandgap shield.
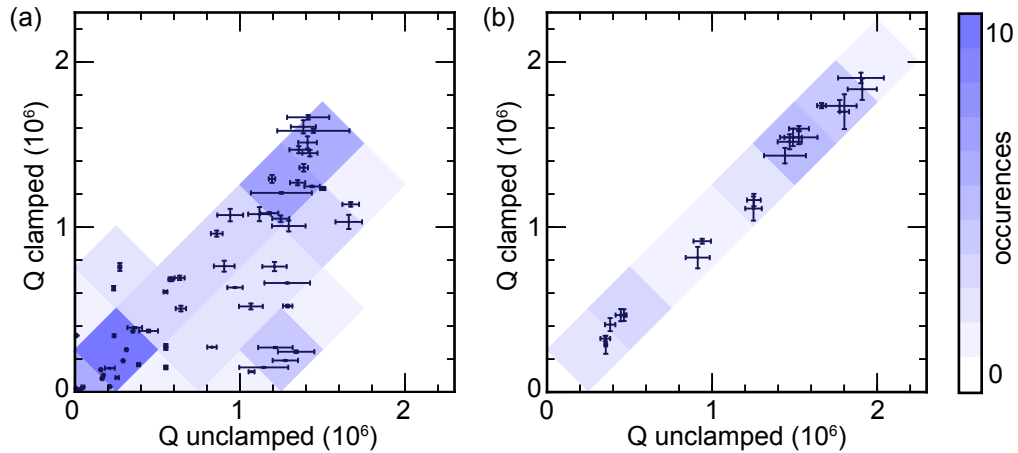

Fig. 7. The quality factors for the devices bolted firmly down, compared to the quality factors of the free-standing devices. The 77 mechanical modes are distributed among 7 devices, all three phononic structures (Fig. 1), different membrane sizes, and mode numbers. We distinguish between membrane modes (a) outside and (b) inside phononic bandgaps.

6. Discussion and outlook

We have shown that the quality factor of the membrane modes can be rendered virtually un-affected by the clamping, and resonant modes of the frame, which indicates that losses due to phonon tunneling into the environment have been eliminated. Still, not all membrane modes reach the highest quality factors ($\sim 2 \times 10^6$). We attribute this lack of full reproducibility to fabrication imperfections. Indeed, we have observed defects and contaminants on the membranes of several devices used for the measurements presented here. We thus strive to improve fabrication and cleaning protocols.

The highest quality factors are expected to be limited by a membrane-internal dissipation mechanism. Assuming constant intrinsic losses it can thus be expected [17] that higher quality factors can be achieved by altering the dimensions of the membrane resonators. For membrane modes with small mode indices the quality factors are proportional to the ratio of the resonator dimensions, $Q \sim L/h$, where L is the side length of the membrane and h is the thickness. Thus by increasing the size of the membranes and / or using thinner SiN layers, we can achieve higher Q-factors.

One indication of the dominating role of the internal dissipation mechanism comes from a smooth and systematic increase of quality factors when the devices with the highest Q's are cooled to cryogenic temperatures. In a preliminary study, we have cooled two samples using a ^{4}He flow cryostat, providing a high-vacuum below 3×10^{-6} mbar, and a cold finger that can be cooled to 8 K. For this study, we have fabricated a sample holder from oxygen-free, high thermal conductivity (OFHC) copper, which tightly clamps the sample, alongside a spacer and a piezoelectric actuator, in a similar fashion as described before (cf. Section 4). Figure 8 shows the result obtained on one sample. We have reached a quality factor above 5×10^6 for 4 different in-bandgap modes, distributed among two devices.
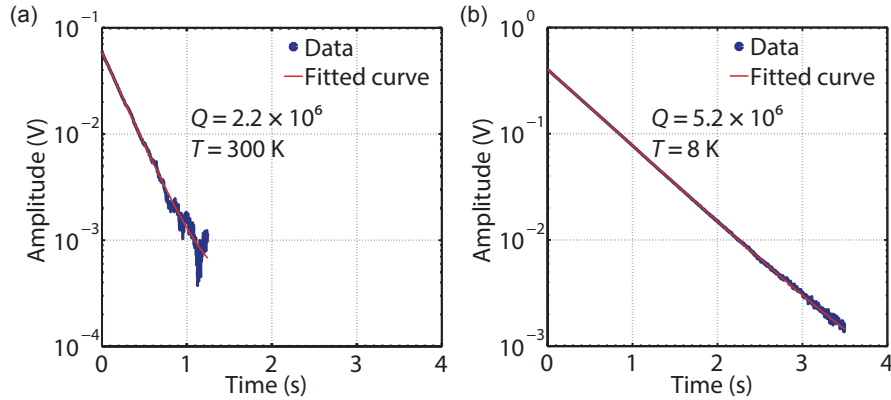

Fig. 8. Results of two ringdown measurements used to determine the quality factor of a in-bandgap (2,2) mode for a cross structure device measured at 300 K (a) and 8 K (b). The frequencies are $f = 2.81 \times 10^6$ Hz and $f = 2.73 \times 10^6$ Hz at 300 K and 8 K, respectively. The vacuum pressure for the room temperature measurement is $\sim 5 \times 10^{-7}$ mbar. The membrane size is $L \sim 285$ μm.

The detailed temperature dependence, the underlying dissipation mechanisms [16, 18, 20] and the associated maximum quality factors will be subject of a future study. Furthermore, we believe that the patterning of the silicon substrate will not affect the thermal properties of our devices. While phononic crystals structure can affect the heat flow in materials, the length scales for such periodic structures is typically on the order of tens of nanometers [24], several orders of magnitude below our structures.

Finally, looking back at Fig. 2, it is interesting how different the features of various phononic structures can be. This raises the question whether it is possible to tailor phononic crystal structures with certain features (e.g. number, position and size of bandgaps). The complexity of the band diagrams and the many possible choices for the geometry of a unit cell call for an adequate optimization strategy. Therefore, we have explored the potential of a genetic algorithm, defining the fitness function F to be optimized as the relative size of the bandgap $F \equiv \Delta f / f_c$.
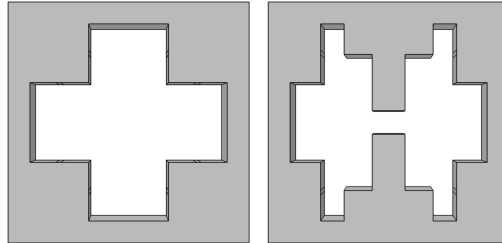
Fig. 9. Unit cell geometries found by genetic optimization. The cross structure (left) and the new geometry (right) have bandgap sizes of ~ 540 kHz and ~ 170 kHz, centered around ~ 2.6 MHz and ~ 1.1 MHz, respectively.

The geometry of the phononic structure's unit cell was parametrized by dividing it into a square grid, which is associated with a binary matrix. The value of each matrix element dictates whether in a given grid point there should be silicon or no silicon. This approach accommodates the requirements set by our experimental and fabricational constraints. In case of a 4-fold symmetric unit cell, the two solutions with the highest fitness found were the cross structure and a new, "walnut"-like geometry (see Fig. 9). Once a suitable geometry has been found, one can employ a different optimization method, such as simulated annealing, to optimize the dimensions of the unit cell for a given geometry.

7. Conclusion

In summary, we have here presented a systematic approach in suppressing clamping losses in high-Q silicon nitride resonators, by means of phononic structure shielding. We have demonstrated the suppression through driven response measurements of the silicon structures, as well as a study of the mechanical quality factors of seven devices in two different mounting configurations (firmly clamped frame and free-standing sample). The suppression of clamping losses enables us to tightly clamp our samples to the cryostat cold finger, thus ensuring good thermalization of the membrane resonators. In that manner, we have reached a quality factor of 5.2×10^6 with a sample tightly bolted to the 8K-cold finger of a cryostat. Our results demonstrate that losses associated with mounting of mechanical resonators can effectively be eliminated by patterning the substrate material.

Acknowledgments